RSC Advances

PAPER

View Article Online
View Journal | View Issue

Cite this: *RSC Adv.*, 2021, **11**, 4186

Flexible and wearable strain sensor based on electrospun carbon sponge/polydimethylsiloxane composite for human motion detection†

He Gong,[ab] Chuan Cai,[b] Hongjun Gu,[b] Qiushi Jiang,[c] Daming Zhang*[a] and Zhiqiang Cheng*[c]

Flexible and wearable strain sensors have attracted considerable attention due to their potential applications in human motion detection. In this work, the as-fabricated strain sensor was obtained by encapsulation of electrospun carbon sponge (CS) with polydimethylsiloxane (PDMS). The formation mechanism of the self-assembled sponge has been explored. Meanwhile, the piezoresistive properties and the strain sensing mechanism of the CS/PDMS sensor were investigated. The results showed that the as-fabricated CS/PDMS sensor had high piezoresistive sensibility with a maximum gauge factor up to 130.49, superior stability and fast response to various cyclic loading with a tensile strain from 0% up to 40% and a tensile speed range of 2–18 mm min^{-1}. Finally, all the superior performances endow the sensor with abilities to precisely detect pronunciation, human palm motion, wrist joint motion, elbow joint motion, and finger motion in real-time. These results indicate that the strain sensor based on the CS/PDMS could have promising applications in flexible and wearable devices for human motion detection.

Received 24th October 2020
Accepted 23rd November 2020

DOI: 10.1039/d0ra09070k

rsc.li/rsc-advances

1. Introduction

In recent years, flexible and wearable strain sensors for human motion detection,[1] intelligent electronic skin,[2] and human–machine interfaces[3] have drawn considerable attention. For piezoresistive strain sensors, the fundamental sensing mechanisms were presented,[4] based on the tunneling effect,[5] the disconnection mechanism,[5,6] as well as the crack propagation mechanism.[5,7,8] For piezoresistive sensors, which can detect variations of resistance signal in response to mechanical deformation or external stimuli applied onto the sensors, are highly attractive due to their simple fabrication, low cost, fast response, and wide detection range.

In order to achieve high sensitivity, flexible strain sensors have been reported based on conductive sponge which is infiltrated with elastic polymer.[4,9–11] In general, various expensive conductive materials such as metal nanoparticles and nanowires,[12,13] graphene,[10] and reduced graphene,[9] and complicated process methods, including chemical vapor deposition (CVD),[14] template,[15] three-dimensional (3D)-printing,[16] and so on, are used to construct those 3D conductive sponges, which may limit their widespread practical applications.

Electrospinning is a viable, cheap yet versatile way to fabricate ultrathin fibers with diameters in the range of nanometers to micrometers. Electrospinning is usually applied to fabricate two-dimensional (2D) non-woven mats.[17] And electrospinning is also powerful in assembly of 3D fibrous polymer sponge.[18,19] Recent studies show that electrospun carbon fibers can be used as a supercapacitor electrode and absorber for selective removal and recovery of oils and organic solvents due to its high conductivity, high porosity and low density.[20,21] However, only a few works have reported the use of electrospun carbon sponge for wearable sensor applications.[22] To the best of our knowledge, there have been no researchers reported that a strain sensor based on electrospun carbon sponge has been used to measure tensile strains.

The most commonly employed elastic polymer is PDMS.[4] Meanwhile, PDMS is a kind of silicone-based elastomers with nice flexibility as matrix of piezoresistive composite that has attracted wide interest, due to its excellent biocompatibility, great thermal stability, high elastic elasticity, as well as fast response speed.[4,23]

In this work, we report a flexible and wearable strain sensor composed of CS infiltrated with PDMS elastomer. And CS was obtained by additive anhydrous aluminum chloride ($AlCl_3$) into electrospinning solution for electrospinning, then produced sponge-like 3D membranes for further carbonization synthesis. The formation mechanism of the self-assembled sponge has been explored. Meanwhile, the piezoresistive properties and the

[a]State Key Laboratory of Integrated Optoelectronics, College of Electronic Science and Engineering, Jilin University, 2699 Qianjin Street, Changchun 130012, China. E-mail: zhangdm@jlu.edu.cn

[b]College of Information Technology, Jilin Agricultural University, 2888 Xincheng Street, Changchun 130118, China

[c]College of Resources and Environment, Jilin Agriculture University, 2888 Xincheng Street, Changchun, 130118, China. E-mail: czq5974@163.com

† Electronic supplementary information (ESI) available. See DOI: 10.1039/d0ra09070k

strain sensing mechanism of the CS/PDMS sensor were investigated. The results showed that the as-fabricated CS/PDMS sensor had high piezoresistive sensibility with a maximum gauge factor of 130.49, superior stability and fast response to various cyclic loading with a tensile strain from 0% up to 40% and a tensile speed range of 2–18 mm min^{-1}. Moreover, human motions including pronunciation, human palm motion, wrist joint motion, elbow joint motion, and finger motion were successfully monitored with CS/PDMS sensor.

2. Materials and methods

2.1. Materials

Polyacrylonitrile (PAN, M_W = 150 000) powder, *N*,*N*-dimethylmethanamide (DMF, 99.8%), anhydrous aluminum chloride ($AlCl_3$, 99.8%) were purchased from Aladdin Chemical Co., Ltd. (China). PDMS (SYLGARD 184 Silicone Elastomer Kit) was purchased from Dow Corning Corp. All chemicals were used as received and underwent no further treatment.

2.2. Preparation of electrospun carbon sponge (CS)

First, the uniform PAN solution (12 wt%) was obtained by magnetic stirring PAN powder and DMF for 6 h in 60 °C water bath. Then, 0.3 g of $AlCl_3$ was added into the 12 wt% PAN solution, followed by magnetic stirring for 3 h in 50 °C water bath. Afterward, the precursor solution was filled in a syringe with a metal spinneret. During electrospinning, the applied voltage, the feed rate of precursor solution, and nozzle-collector distance were controlled at 15 kV, 0.5 mL h^{-1}, and 20 cm, respectively. A grounded steel roller (length: 5 cm; diameter: 7 cm) was used as a collector, and the steel roller rotary speed was limited at 120 rad min^{-1}. After electrospinning, a nonwoven porous sponge was obtained.

The as-obtained sponge was firstly dried in an air cycling oven at 60 °C for 3 h and then the oxidative stabilization of the sponge was carried out at the same condition but the temperature and time change to 210 °C and 2 h, respectively. Subsequently, carbonization was performed in a tube furnace at 1050 °C for 1 h under a nitrogen atmosphere to convert the sponge into carbon sponge (CS), and the temperature was increased at a rate of 5 °C min^{-1}. Finally, the CS was obtained after the tube furnace being cooled down to room temperature. Please note that carbonization treatment is a process that converts the PAN precursor fiber to carbon fiber, and the carbonization process will not be 100%.[24,25]

2.3. Assembly of strain sensor

The CS strain sensor was fabricated by simply encapsulation of CS with PDMS, it means that CS is fully infiltrated with PDMS or CS embedded in PDMS. Firstly, the obtained CS was cut into pieces (30 mm × 10 mm × 2 mm). Then, two sheets of copper foil electrode were glued with conductive silver paste at the two sides of the CS pieces. Finally, the PDMS liquid base and crosslinker were homogeneously mixed in a mass ratio of 10 : 1 and poured on the surface of the CS with electrodes inside a mold, which was subsequently degassed in a vacuum chamber for 20 min.[26] By removing air bubbles, the PDMS can fully coating the CS. To ensure that the polymerization process is complete. Then heat to 80 °C for 3 hours, when PDMS is fully cured, the excess PDMS will be carefully cut off. Liu *et al.* studied the effect of temperature on the mechanical properties of PDMS, indicating that at low temperatures, the mechanical properties are independent of heating time, while higher heating temperatures leads to produce lower mechanical strength.[27] To make the CS/PDMS sensor obtain proper mechanical strength, the heating temperature reached 80 °C and kept for 3 hours.

2.4. Characterization

The morphologies of CS were performed by scanning electron microscopy (SEM, SHIMADZUX-550). Carbonized fibers corresponding element mapping was performed by energy dispersive spectroscopy (EDS, SHIMADZUX-550 Scanning Electron Microscope Accessories). The tensile tests of the CS/PDMS strain sensor were measured by STD100 microcomputer-controlled electronic universal testing machine (RicKs Measurement and Control Co., Ltd.), while the electrical signals were measured by Keysight B2902A Precision Source/Measure Unit (KEYSIGHT B2902A).

3. Results and discussion

Fig. 1a displays a schematic of fabrication of the CS/PDMS strain sensor *via* dry and oxidative stabilization of the PAN–aluminum sponge and then carbonization, followed by encapsulation CS with PDMS. The fracture surface of the CS/PDMS composite is shown in Fig. S1,† carbon fibers are loosely spread in PDMS and the CS's 3D structure had been well maintained after encapsulation by PDMS. After a series of heat treatments, the $AlCl_3$ was converted into Al_2O_3. The Al_2O_3 was homogeneously dispersed all over the carbonized fibers as shown in EDS mapping images of Fig. S2.† Fig. 1b and c shows the morphology of the 3D CS fibers at different magnifications. And the obtained CS consisted of fluffy, loosely packed fibers, and the interwove fibers with an average diameter of 374 nm, and a narrow fiber diameter distribution. Meanwhile, the CS also exhibited excellent flexibility while being compressed and folded (Video S1†). Fig. 3c displays both in-focus and blurry, out-of-focus fibers, which is proof of the 3D structure of the CS.[28]

In this work, the PAN–aluminum sponge is directly prepared by electrospinning. The electrospinning precursor solution is one of the most important decisive factors that have a significant effect on the formation of 3D fibers.[28] $AlCl_3$ was used as an ion (Al^{3+}) source for building 3D nanostructures.[22,29] By adding an appropriate amount of $AlCl_3$ (*e.g.*, 0.3 g) into the PAN solution and after full of mixing, the viscosity of the precursor solution was increased.[30] And with the viscosity increased, causing an improvement in the precursor solution spinning ability as well as fiber solidification speed. In addition, during electrospinning, aluminum-ions are polarized easily under the action of a strong electric field, thereby leading to the repulsive force increases in and among the charged Taylor cones/fibers, which will also beneficial the fiber solidification. The morphology of nanofiber is easily affected by the distance between nozzle to collector, the average nanofiber diameters tend to decrease with the distance increase, as the jet elongation

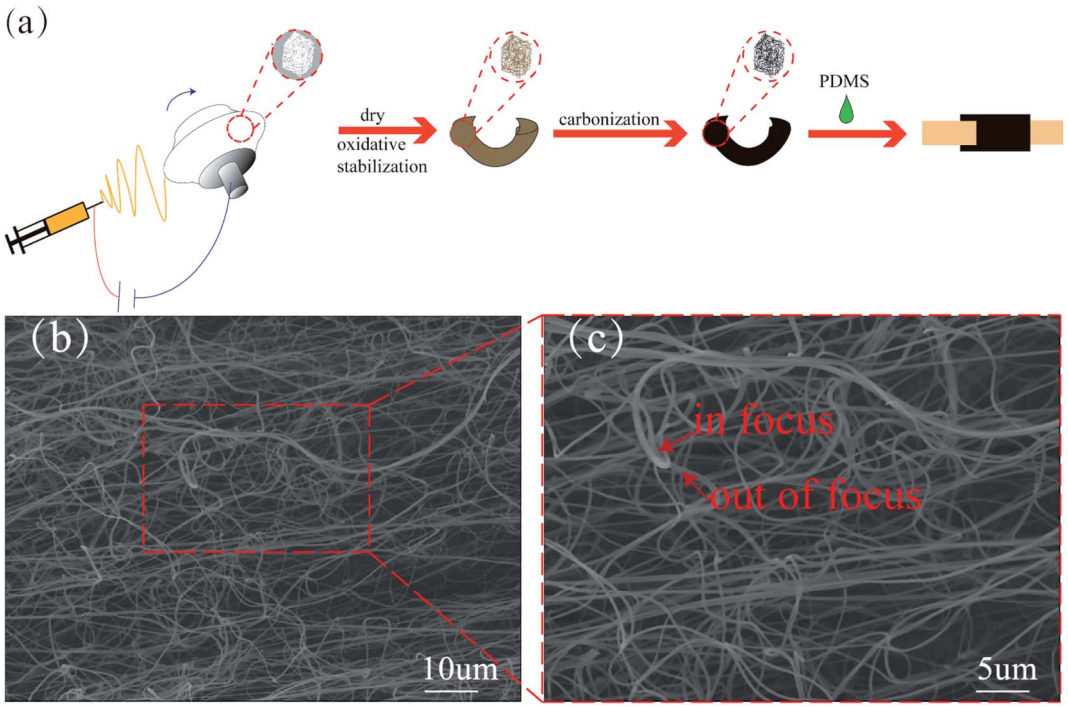

Fig. 1 (a) Schematic illustration showing the fabrication process of the CS/PDMS strain sensor. (b) The SEM of the carbon sponge fibers. (c) The zoomed-in section of (b).

time increases.[19] But a decrease in nanofiber diameter and have no obvious influence in nanofiber diameter with increasing the distance between needle and collector were also reported in the literature.[31,32] In a published study by Jalili R. *et al.*, by electrospinning of PAN/DMF solution of 15 wt% concentration, the authors found that at 5 and 7.5 cm between nozzle to collector, the collected nanofiber was mostly wet. When the distance at 15 cm, the nanofiber was completely dry and stabilized.[33] This means that the deposited fibers can be rapid solidification, in this case, the appropriate increase in distance is conducive to fibers to build 3D networks. Besides, the choice of electrospinning solution is a decisive element on the formation of 3D networks.[28] And solvent is one of the main contributors to electrospinning solution. Ucar Nuray, *et al.* found that PAN nanofibers produced from DMF solvent had smaller fiber diameters than nanofibers produced from dimethylsulfoxide (DMSO) and *N*-methylpyrrolidone (NMP) solvents, after electrospinning, DMSO and NMP did not evaporate, while DMF evaporated rapidly and the deposited fibers can be rapid solidification.[34] Under this condition, choosing the appropriate solvent is beneficial to the solidification of the fiber. As a result, DMF was used as solvent in this work. Finally, the rapidly solidified fibers can support the subsequently deposited fibers and through the repetitive the process of deposition and support, nanofiber layers were gradually increased and a porous PAN–aluminum sponge will be obtained. And the central part of the obtained sponge is a little thicker than the outer part due to the distribution of the electric field.[17,30]

In Fig. 2, it is obvious that the relative change of the resistance (RCR, $\Delta R/R_0 = (R_c - R_0)/R_0$, where R_0 and R_c are the resistance without and with applied tensile strain, respectively.) of CS/PDMS sensor monotonically increases with the increasing tensile strain. The RCR increased rapidly more than 100 after being applied with an 8.0% tensile strain, and even in a relatively low strain of 2.9–5.0%, the values of RCR can be also held in the range of 20–50. This demonstrates that the CS/PDMS sensor has an obvious response to the external tensile strain, which is also beneficial practical applications of the sensor. Here, the gauge factor (GF) is defined as $\delta(\Delta R/R_0)/\delta\varepsilon$, where ε stands for the strain, measuring the sensitivity of the strain sensor. Meanwhile, as shown in Fig. 2, according to the variation of slopes, three regions can be obtained. So the GF of the CS/PDMS sensor in the range of 0–30%, 30–50%, 50–60% calculated is 13.23, 43.16, and 130.49, respectively. The GF of the CS/PDMS sensor at a high tensile strain range (50–60%) is around 10 and 3 times larger than that at low (0–30%) and middle (30–50%) tensile strain range. And when the applied tensile strain is less than 30%, the GF is calculated to be 13.23, which is much higher than that of conventional strain sensors based on metals (GF around 2).[35] Li *et al.* prepared a carbon waste paper sponge/PDMS composite for strain sensor applications and under tension the obtained RCR value much lower than reported in this work.[36] And the obtained carbonized cellulose fibers are belt-like with a width around 10 μm. In this work, the 3D CS fibers with an average diameter of 347 nm, which has a smaller diameter than belt-like fibers. The smaller diameter of fiber will provide more fibers contact sites.[37] And the interwove fibers built the 3D CS structure as well as contact sites, so the 3D CS will have more contact sites. Remarkably, when the CS/PDMS sensor under tension more contact sites will be destroyed. This will cause a larger RCR value. Besides, the rough surface of fiber tends to improve the adhesion between fibers and matrix.[38] And the belt-like cellulose fibers have rough

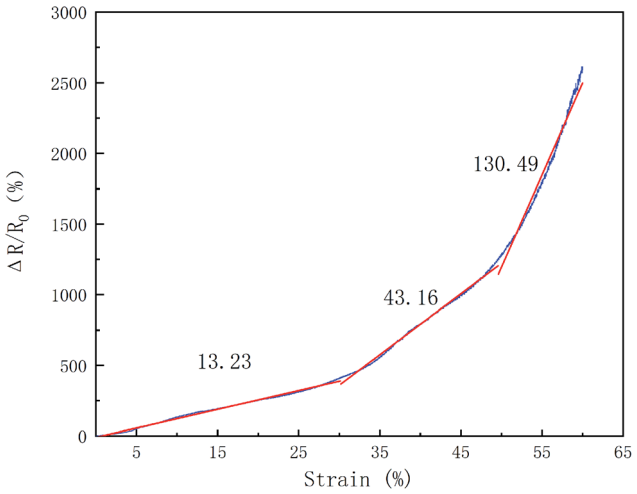

Fig. 2 The RCR response of the CS/PDMS sensor as a function of the applied tensile strain at the rate of 1 mm min^{-1}.

surface tending to have more adhesion with PDMS, this is not conducive to the slide of fibers during tensile strain, which will cause a lower RCR value. Table 1 shows the comparison of RCR value, GF, and other versatile properties of various strain sensors based on carbon fibers. Obviously, the CS/PDMS sensor exhibits both a large sensing range and relatively high GF. The integration of a wide tensile strain range and high GF of CS/PDMS sensor, making it can be used as a strain sensor with a wide range to detect human motions.

To understand the mechanism of the CS/PDMS sensor, a schematic of the internal structural change of the sensor with and without applied tensile strain is proposed in Fig. 3. The structure of the porous 3D carbon sponge in the PDMS as the key sensing element is presented. The 3D conductive porous structural network is formed by the interconnected carbon fibers, as shown in the SEM images (Fig. 1b and c). The mechanism of a resistance change is related to the three phases of tensile strain: breaking phase, sliding phase, and disconnecting phase, which are closely associated with the variation of the CS structure. At the initial phase, the interwove fibers of CS encapsulation by PDMS are continuous (Fig. 3a). In the breaking phase ($0 < \varepsilon < 30\%$, Fig. 3b), with the tensile strain increased, the interwove fibers of CS begin to break into short fibers, resulting in the breakage of initial continuous conductive pathways and rapid increase of the resistance of the conductive CS. In the sliding phase ($30\% < \varepsilon < 50\%$, Fig. 3c), with the further increase of applied tensile strain, leading to the result that more fibers may be broken into short fibers. Meanwhile, the shortened fibers may slide with each other and decrease the effective contact area between the interwove fibers of CS, leading to an increase of the contact resistance between interwove fibers of CS. By the synergistic action of fibers break and slide with each other, the resistance sharply increased. In the disconnecting phase ($50\% < \varepsilon < 60\%$, Fig. 3d), when the interwove fibers of CS under higher tensile strain, the shortened fibers are stretched over the sliding limit, and the dominated mechanism is the disconnect of carbon fibers in the PDMS matrix. As the carbon fibers are much stiffer than the PDMS elastomer, when the sensor under large tensile strain, discontinuousness start to appear in the 3D conductive porous structural network, resulting in a significant increase in the

Table 1 Comparison of RCR value, GF, and other versatile properties of various strain sensors based on carbon fibers

Materials	Sensing range	RCR	GF	Reference
Carbon waste paper sponge/PDMS	25%	>40	1.78	36
Carbon paper/PDMS	20%	>150	25.3	39
Carbon nanofibers/polyurethane	300%	>11 000	40	40
CS/PDMS	60%	>2500	130.49	This work

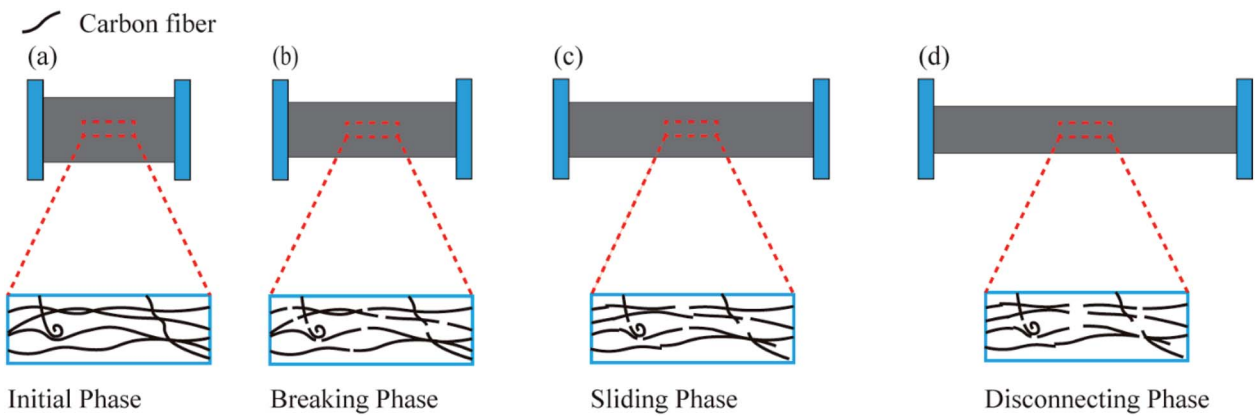

Fig. 3 Schematic evolutions of the internal structural change of the CS/PDMS sensor with and without applied tensile strain. (a) Initial phase, (b) breaking phase, (c) sliding phase, (d) disconnecting phase.

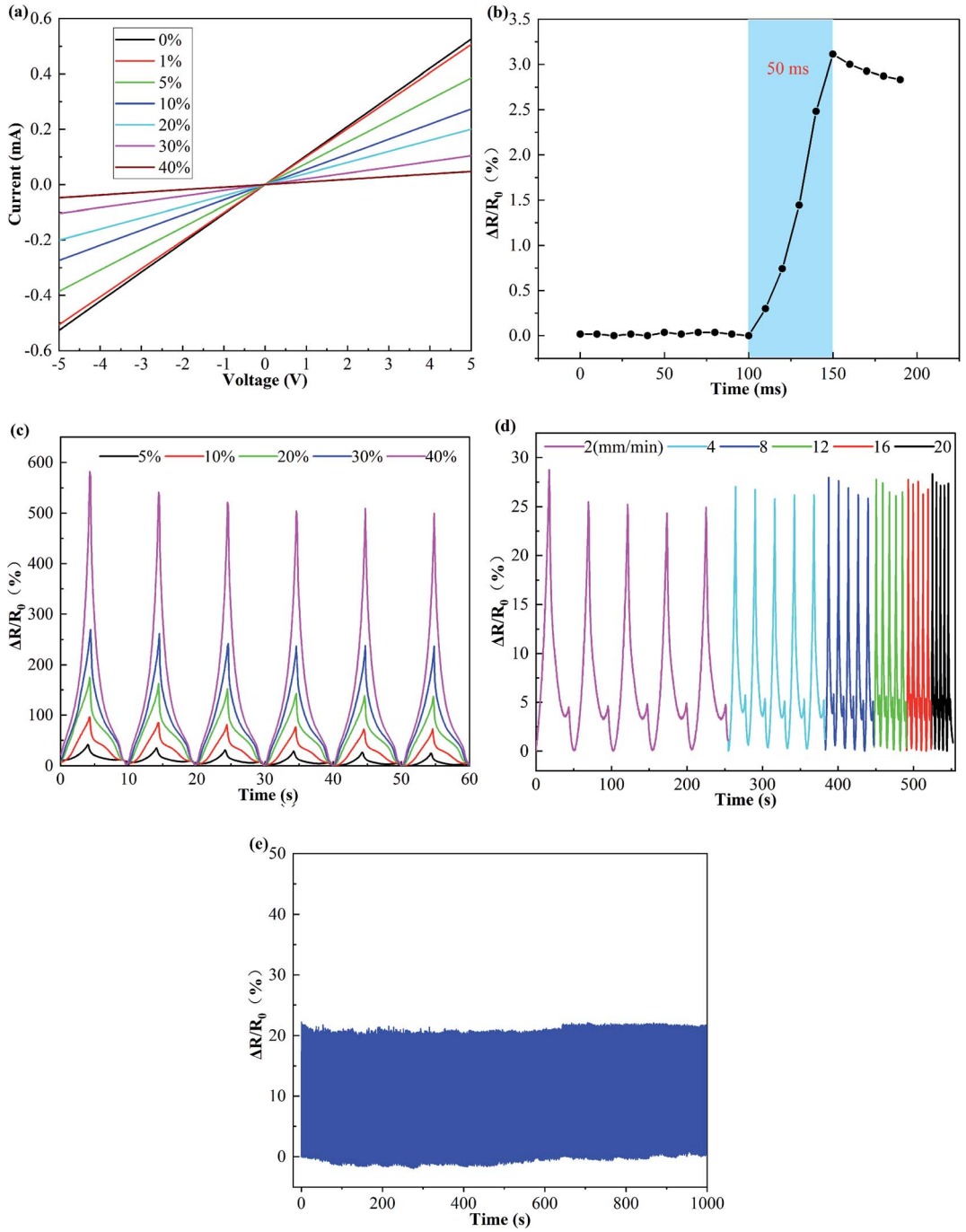

Fig. 4 (a) *I–V* curves of CS/PDMS strain sensor with different tensile strains. (b) The response time of the CS/PDMS strain sensor. (c) RCR response of the CS/PDMS strain sensor to cyclic tension at various tensile strains cycles. (d) RCR response of the strain sensor with different tensile speed (2, 4, 6, 8, 12, 14, 16 and 20 mm min^{-1}) under a tensile strain of 5%. (e) Durability test of the CS/PDMS sensor at a frequency of 1 Hz with the 5% tensile strain peak for 1000 cycles.

resistance. This phenomenon has also been reported in previous literatures.[40–42]

Fig. 4a shows the current–voltage (*I–V*) curves for CS/PDMS sensor with different tensile strains. The resistance of CS/PDMS sensor rises with the increasing tensile strain (from 0% to 40%) at a given voltage. It is clear that these linear *I–V* curves confirm excellent ohmic behavior of CS/PDMS sensor, demonstrating that the CS/PDMS sensor possesses good conductivity in a wide tensile stain range from 0% to 40%.

To investigate the response time of the CS/PDMS strain sensor, dynamic tensile strain inputs have been applied as shown in Fig. 4b. It is noting that the response time was only 50 ms under 0.5% tensile strain and at a high tensile rate of 500 mm min^{-1}. The fast response time guarantees a fast response to

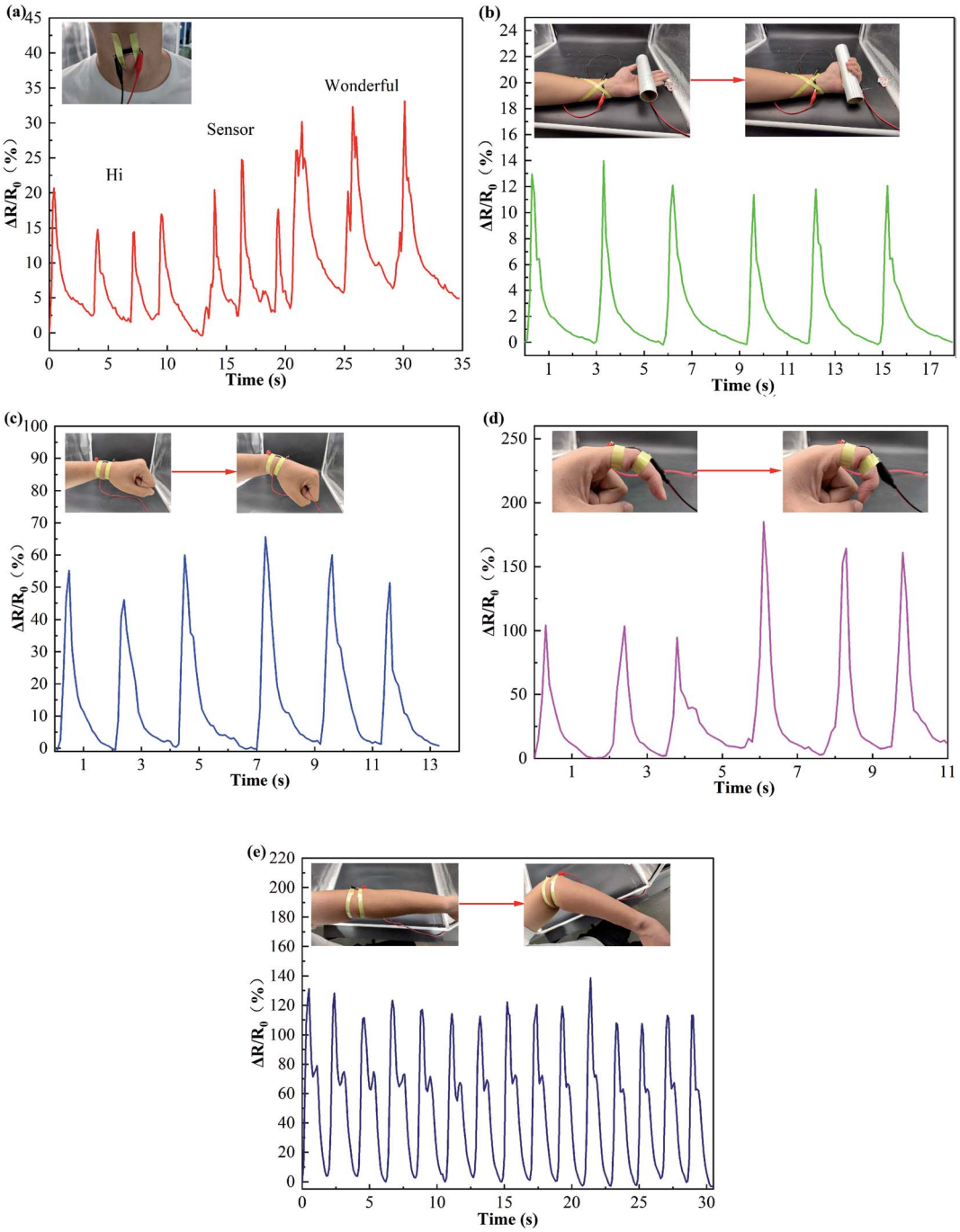

Fig. 5 application of the CS/PDMS strain sensor for the real-time human motion detection: response of the strain sensor to cycle motion of (a) pronunciation "hi", "sensor", and "wonderful", respectively, (b) human palm, (c) wrist joint, (d) finger and (e) elbow joint (inset show photograph of a strain sensor attached on (a) pronunciation, (b) human palm, (c) wrist joint, (d) finger, and (e) elbow joint of a volunteer).

strain stimulus. Fig. 4c shows the RCR responses at various tensile strains cycles. It is important to first note the stability of the response produced under cyclic tensile strain, the RCR response curves almost exhibit no obvious variation from the first to final cycle, indicating excellent repeatability of the prepared CS/PDMS strain sensor. Second, as the peak strain increases from 5% to 40%, the magnitude of the RCR response also remains stable improvement from 25% to 581%. Considering that the strain rate-dependence is one of the important characteristics for a sensor, the response of the CS/PDMS strain sensor under a tensile speed range of 2–18 mm min^{-1} is herein investigated, as shown in Fig. 4d. And all response signals closely follow the input strains and are almost no frequency dependence, indicating that the strain sensor is reliable and has a fast response in a wide range of loading frequencies. Meanwhile, it can be observed that the RCR

generally increased when the tensile force was applied. This typical behavior can be defined as positive strain effect.[43] Moreover, during the RCR decreased with decreasing strain, shoulder peaks are also observed during these cycles, this shoulder peak can be defined as negative strain effect,[44] which is regarded as an indication of the competition between destruction and reconstruction of conducting pathways during dynamic loading.[41,44] The durability of the CS/PDMS strain sensor is another key feature for its practical applications, the strain sensor within 1000 tensioning–releasing cycles at a frequency of 1 Hz with 5% tensile strain, as shown in Fig. 4e. The RCR of the CS/PDMS strain sensor was nearly invariant during 1000 stretching–releasing cycles and exhibited excellent stability and durability. All the results indicated that the CS/PDMS strain sensor possesses superior performance and excellent stability.

Due to the combined advantages of good sensitivity, reliability, and durability, the CS/PDMS strain sensor was used to monitor various human motions to demonstrate its potential as wearable electronic devices. Fig. 5a shows the flexible CS/PDMS strain sensor attached to the throat of a volunteer, when the volunteer says a monosyllabic word "hi", a dissyllabic word "sensor", and a polysyllabic word "wonderful" respectively, and the response signal curves of each word have distinctive and repeatable characteristic peaks, indicating the CS/PDMS strain sensor potential for application of voice recognition. As shown in Fig. 5b, by attaching the CS/PDMS strain sensor onto the inside of wrist joint could precisely supervise the motions of the palm. As displayed in Fig. 5c, by attaching the CS/PDMS strain sensor onto the back of wrist joint, the real-time finger bending states signals were recorded (Video S2†). The results show that the CS/PDMS strain sensor may be useful for human medical applications in the future. Fig. 5d displays the CS/PDMS stain sensor was attached on index finger could be precisely identified by bending deformation under different angles (Video S3†). The CS/PDMS sensor response signal increased with the increase of bending angles of the index finger and the corresponding response signals are distinguishable under different index finger bending angles. Such results suggest that the CS/PDMS strain sensor can be potential to track the behavior of the fingers bend angles. As can be seen in Fig. 5e, the CS/PDMS strain sensor was fixed in the joint of elbow to monitor the large-scale human motions, it can be clearly seen that the RCR periodically rises with the elbow bending, and drops with the elbow unbending, which exhibited good responsivity and reproducibility. All the testing results demonstrate that the CS/PDMS sensor can be used in human motion detection.

4. Conclusions

In summary, a flexible and wearable strain sensor based on PDMS encapsulation electrospun CS has been fabricated. The formation mechanism of the self-assembled sponge has been explored, in which $AlCl_3$ was used as an ion (Al^{3+}) source for building 3D nanostructures. The structure of the porous 3D carbon sponge in the PDMS as the key sensing element is presented. The mechanism of a resistance change is related to three phases of tensile strain: break phase, sliding phase, and disconnecting phase. In this work, the CS/PDMS strain sensor could achieve a high GF of 13.23, 43.16, and 130.49 within the tensile strain of 0–30%, 30–50%, 50–60%, respectively. Furthermore, the CS/PDMS strain sensor performs fast response (50 ms), high stability (1000 cycles), and a wide tensile speed range of 2–18 mm min^{-1}. As a result, the CS/PDMS sensor can precisely detect various human motions, such as pronunciation, human palm motion, wrist joint motion, elbow joint motion, and finger motion, indicating its promising for practical application in flexible and wearable devices that would have a promising application in human-motion detecting.

Conflicts of interest

There are no conflicts to declare.

Acknowledgements

This research was funded by The People's Republic of China Ministry of Science and Technology under grant number 2018YFF0213606-03, the Science and Technology Department of Jilin Province under grant numbers 20160623016TC, 20200402006NC, the Science and Technology Support Project for Key Industries in Southern Xinjiang under grant number 2018DB001, and the Development and Reform Commission of Jilin Province under grant number 2019C021. Jilin Province Science and Technology Development Project under grant numbers 20200708066YY and 20200403166SF.

Notes and references

1 X. Fang, J. Tan, Y. Gao, Y. F. Lu and F. Z. Xuan, *Nanoscale*, 2017, **9**, 17948–17956.
2 Q. Hua, J. Sun, H. Liu, R. Bao and Z. L. Wang, *Nat. Commun.*, 2018, **9**, 1–11.
3 Y. Li, Y. A. Samad, T. Taha, G. Cai, S. Y. Fu and K. Liao, *ACS Sustainable Chem. Eng.*, 2016, **4**, 4288–4295.
4 L. Duan, D. R. D'Hooge and L. Cardon, *Prog. Mater. Sci.*, 2019, **114**, 100617.
5 Y. Li, S. Wang, Z.-C. Xiao, Y. Yang, B.-W. Deng, B. Yin, K. Ke and M.-B. Yang, *J. Mater. Chem. C*, 2020, **8**, 4040–4048.
6 G.-J. Zhu, P.-G. Ren, H. Guo, Y.-L. Jin, D.-X. Yan and Z.-M. Li, *ACS Appl. Mater. Interfaces*, 2019, **11**, 23649–23658.
7 H. Liu, Q. Li, Y. Bu, N. Zhang and C. Shen, *Nano Energy*, 2019, **66**, 104143.
8 J. Gao, B. Li, X. Huang, L. Wang, L. Lin, H. Wang and H. Xue, *Chem. Eng. J.*, 2019, **373**, 298–306.
9 X. Jiang, Z. Ren, Y. Fu, Y. Liu, R. Zou, G. Ji, H. Ning, Y. Li, J. Wen and H. J. Qi, *ACS Appl. Mater. Interfaces*, 2019, **11**, 37051–37059.
10 Y. Pang, H. Tian, L. Tao, Y. Li, X. Wang, N. Deng, Y. Yang and T.-L. Ren, *ACS Appl. Mater. Interfaces*, 2016, **8**, 26458–26462.
11 X.-G. Yu, Y.-Q. Li, W.-B. Zhu, P. Huang, T.-T. Wang, N. Hu and S.-Y. Fu, *Nanoscale*, 2017, **9**, 6680–6685.

12 D. Kang, P. V. Pikhitsa, Y. W. Choi, C. Lee, S. S. Shin, L. Piao, B. Park, K.-Y. Suh, T.-i. Kim and M. Choi, *Nature*, 2014, **516**, 222–226.
13 B.-U. Hwang, J.-H. Lee, T. Q. Trung, E. Roh, D.-I. Kim, S.-W. Kim and N.-E. Lee, *ACS Nano*, 2015, **9**, 8801–8810.
14 N. Luo, Y. Huang, J. Liu, S. C. Chen, C. P. Wong and N. Zhao, *Adv. Mater.*, 2017, **29**, 1702675.
15 C. Wang, Y. Ding, Y. Yuan, A. Cao, X. He, Q. Peng and Y. Li, *Small*, 2016, **12**, 4070–4076.
16 S. Z. Guo, K. Qiu, F. Meng, S. H. Park and M. C. McAlpine, *Adv. Mater.*, 2017, **29**, 1701218.
17 B. Sun, Y.-Z. Long, F. Yu, M.-M. Li, H.-D. Zhang, W.-J. Li and T.-X. Xu, *Nanoscale*, 2012, **4**, 2134–2137.
18 B. Sun, Y. Long, H. Zhang, M. Li, J. Duvail, X. Jiang and H. Yin, *Prog. Polym. Sci.*, 2014, **39**, 862–890.
19 Y. Wang, W. Li, Y. Zhou, L. Jiang and F. Zhou, *J. Mater. Sci.*, 2020, **55**, 12592–12606.
20 F. Lai, Y. Huang, L. Zuo, H. Gu, Y.-E. Miao and T. Liu, *J. Mater. Chem. A*, 2016, **4**, 15861–15869.
21 M. H. Tai, B. Y. L. Tan, J. Juay, D. D. Sun and J. O. Leckie, *Chem.–Eur. J.*, 2015, **21**, 5395–5402.
22 Z. Han, Z. Cheng, Y. Chen, B. Li, Z. Liang, H. Li, Y. Ma and X. Feng, *Nanoscale*, 2019, **11**, 5942–5950.
23 M. P. Wolf, G. B. Salieb-Beugelaar and P. Hunziker, *Prog. Polym. Sci.*, 2018, **83**, 97–134.
24 T. H. Ko and L. C. Huang, *J. Appl. Polym. Sci.*, 1998, **70**, 2409–2415.
25 M. S. A. Rahaman, A. F. Ismail and A. Mustafa, *Polym. Degrad. Stab.*, 2007, **92**, 1421–1432.
26 C. W. Schultz, C. L. Ng and H.-Z. Yu, *ACS Appl. Mater. Interfaces*, 2019, **12**, 3161–3170.
27 M. Liu, J. Sun and Q. Chen, *Sens. Actuators, A*, 2009, **151**, 42–45.
28 H.-Y. Mi, X. Jing, B. N. Napiwocki, Z.-T. Li, L.-S. Turng and H.-X. Huang, *Chem. Eng. J.*, 2018, **331**, 652–662.
29 O. Y. Kweon, S. J. Lee and J. H. Oh, *NPG Asia Mater.*, 2018, **10**, 540–551.
30 M. M. Li and Y. Z. Long, *Mater. Sci. Forum*, 2011, **688**, 95–101.
31 C. Zhang, X. Yuan, L. Wu, Y. Han and J. Sheng, *Eur. Polym. J.*, 2005, **41**, 423–432.
32 T. Wang and S. Kumar, *J. Appl. Polym. Sci.*, 2006, **102**, 1023–1029.
33 R. Jalili, S. A. A. Hosseini and M. Morshed, *Iran. Polym. J.*, 2005, **14**, 1074–1081.
34 N. Ucar, N. Kizildag, A. Onen, I. Karacan and O. Eren, *Fibers Polym.*, 2015, **16**, 2223–2236.
35 C. Farcau, N. M. Sangeetha, H. Moreira, B. Viallet, J. Grisolia, D. Ciuculescu-Pradines and L. Ressier, *ACS Nano*, 2011, **5**, 7137–7143.
36 Y.-Q. Li, W.-B. Zhu, X.-G. Yu, P. Huang, S.-Y. Fu, N. Hu and K. Liao, *ACS Appl. Mater. Interfaces*, 2016, **8**, 33189–33196.
37 K. Qi, J. He, H. Wang, Y. Zhou, X. You, N. Nan, W. Shao, L. Wang, B. Ding and S. Cui, *ACS Appl. Mater. Interfaces*, 2017, **9**, 42951–42960.
38 S.-J. Park, M.-K. Seo and H.-B. Shim, *Mater. Sci. Eng., A*, 2003, **352**, 34–39.
39 Y. Li, Y. A. Samad, T. Taha, G. Cai, S.-Y. Fu and K. Liao, *ACS Sustainable Chem. Eng.*, 2016, **4**, 4288–4295.
40 Y. Ding, J. Yang, C. R. Tolle and Z. Zhu, *RSC Adv.*, 2016, **6**, 79114–79120.
41 L. Lin, S. Liu, Q. Zhang, X. Li, M. Ji, H. Deng and Q. Fu, *ACS Appl. Mater. Interfaces*, 2013, **5**, 5815–5824.
42 Z. He, G. Zhou, J.-H. Byun, S.-K. Lee, M.-K. Um, B. Park, T. Kim, S. B. Lee and T.-W. Chou, *Nanoscale*, 2019, **11**, 5884–5890.
43 E. Bilotti, R. Zhang, H. Deng, M. Baxendale and T. Peijs, *J. Mater. Chem.*, 2010, **20**, 9449–9455.
44 S. Salaeh, A. Das, K. W. Stöckelhuber and S. Wießner, *Composites, Part A*, 2020, **130**, 105763.